Linköping University Post Print

Role of stoichiometric and nonstoichiometric defects on the magnetic properties of the half-metallic ferromagnet NiMnSb

Björn Alling, Sam Shallcross and Igor Abrikosov

N.B.: When citing this work, cite the original article.

Original Publication:

Björn Alling, Sam Shallcross and Igor Abrikosov, Role of stoichiometric and nonstoichiometric defects on the magnetic properties of the half-metallic ferromagnet NiMnSb, 2006, Physical Review B. Condensed Matter and Materials Physics, (73), 6, 064418.
http://dx.doi.org/10.1103/PhysRevB.73.064418

Copyright: American Physical Society
http://www.aps.org/

Postprint available at: Linköping University Electronic Press
http://urn.kb.se/resolve?urn=urn:nbn:se:liu:diva-35025

Role of stoichiometric and nonstoichiometric defects on the magnetic properties of the half-metallic ferromagnet NiMnSb

B. Alling,* S. Shallcross, and I. A. Abrikosov
Department of Physics, Chemistry and Biology, University of Linköping, SE-581 83 Linköping, Sweden
(Received 21 October 2005; published 16 February 2006)

The first material to be predicted from first-principles calculations as half-metallic was NiMnSb, and the research on this material has been intense due to its possible applications in spintronics devices. The failure of many experiments to measure spin polarization to more than a fraction of the predicted 100% has partly been blamed on structural defects. In this work a complete first-principles treatise of point defects, including nonstoichiometric antisites, interstitial and vacancy defects, as well as stoichiometric atomic swap defects in NiMnSb, is presented. We find that the formation energies of the defects span a large scale from 0.2 to 14.4 eV. The defects with low formation energies preserve the half-metallic character of the material. We also find that some of the defects *increase* the magnetic moment and thus can explain the experimentally observed increase of magnetic moments in some samples of NiMnSb. Most interesting in this respect are Mn interstitials which increase the magnetic moment, have a low formation energy, and keep the half-metallic character of the material.

DOI: 10.1103/PhysRevB.73.064418 PACS number(s): 75.10.−b, 75.50.Cc, 71.55.−i

I. INTRODUCTION

Research in the field of spin-dependent electronics, spintronics, has been intense in the last decades. One field of research has been the creation of spin-polarized current. In this area the so-called half-metallicity has been a key property. A half-metal is a material where the conduction electrons are 100% spin polarized. This happens because the Fermi level falls into a gap in the spin-down channel while the density of states at E_F has a nonvanishing value for spin-up electrons. The first material that was predicted to be half-metallic was the half-Heusler alloy NiMnSb.[1] A large number of experiments as well as first-principles calculations were performed on this material. Positron annihilation experiments[2] as well as resistivity and magnetic measurements[3–5] support the theory of half-metallicity at low temperatures. Surface- and interface-sensitive techniques like spin valves[6] and tunnel junctions[7] as well as Andreev reflection experiments[8] show a far lower degree of spin polarization. Calculations have shown that surfaces and interfaces with semiconductors in general are not half-metallic.[9] However de Wijs and de Groot[10] showed that using the right semiconductor and growth direction half-metallicity can be restored. One other proposed source of destruction of the 100% spin polarization at the Fermi level is structural defects.[11] Orgassa *et al.*[11,12] used a layer Korringa-Kohn-Rostoker (KKR) technique within the coherent potential approximation to show that some specific stoichiometric atomic swap defects induced spin-down states at the Fermi level at low concentrations. They also reported that the defects should *decrease* the magnetic moment of the material,[12] a result which differs from many experiments which instead show magnetic moments slightly higher than the predicted integer value of $4.00\mu_B$ in ideal NiMnSb.[3,5,13,14] Attema *et al.*[15] later claimed that the most damaging defects were energetically unfavorable and thus should be possible to avoid in state-of-the-art thin-film growth techniques. However, no first-principles calculations have been presented on the effect of nonstoichiometric defects on the properties of NiMnSb. At the same time the effect of nonstoichiometry is interesting due to the difficulty to exactly control the composition of the produced sample. This is so because of differences in the consumption rate of Ni, Mn, and Sb in the melting or growth process and due to the eventual formation of other phases like NiSb.

In this work a complete and systematic first-principles investigation of the six possible intrinsic (only using Ni, Mn, and Sb) antisite defects, three interstitial defects, three vacancies, and 12 atomic swap defects in NiMnSb is performed. The results are presented in terms of formation energy, electronic, and magnetic properties. The work is organized in the following way: in Sec. II we characterize the structure of the material and explain our notation for the defects considered in this work. In Sec. III we report the computational details, in Sec. IV the results of the calculations are reported and discussed, and in Sec. V conclusions are drawn.

II. STRUCTURAL INFORMATION

NiMnSb crystallizes in the $C1_b$ crystal structure consisting of four interpenetrating fcc sublattices with the offsets $A=(0,0,0)$, $B=\left(\frac{1}{4},\frac{1}{4},\frac{1}{4}\right)$, $C=\left(\frac{1}{2},\frac{1}{2},\frac{1}{2}\right)$, and $D=\left(\frac{3}{4},\frac{3}{4},\frac{3}{4}\right)$ with sites occupations A=Ni, B=Mn, C=empty, and D=Sb.

We perform first-principles calculations within the KKR atomic sphere approximation[16,17] (ASA) framework where the C sublattice consists of empty spheres. In this context six kinds of antisite defects are possible as well as three different interstitial defects where Ni, Mn, and Sb, respectively, are present in the vacant position. In addition, three different types of vacancies, at the Ni, Mn, and Sb sublattices, respectively, are treated. When considering the atomic swap defects six types of swaps between species are possible if one also treats the interstitial position as a sublattice occupied by empty species. In principle swaps between atoms at different

 ©2006 The American Physical Society

distances can occur. In this work we consider swaps between the nearest-neighboring (or next-nearest-neighboring depending on swap type) atoms as well as swaps between atoms far away from each other.

We use the following notations for the defects: A defect where an atom of the kind A is sitting on the sublattice that in the perfect crystal is occupied by an atom of kind B is denoted A_B; that is, a Ni atom on the Mn sublattice is denoted $\mathrm{Ni_{Mn}}$. A defect where an atom of type A is placed on the empty sublattice—that is, an interstitial defect—is denoted A_I. A vacancy defect where the position of an atom of type A is vacant is denoted vac_A. Swap defects are denoted in an obvious way where the nearest-neighbor swap is abbreviated nn and the more distant swap is abbreviated dst.

III. COMPUTATIONAL DETAILS

We use the locally self-consistent Green's function (LSGF) method[18,19] to calculate a supercell of 500 atoms consisting of $5\times5\times5$ unit cells making the defect concentration 0.8%. The size of the local interaction zone (LIZ) includes the three nearest-neighbor shells. The lattice constant was kept fixed at the experimental value 5.927 Å^3 in all calculations. The local spin-density aproximation (LSDA) was used for the exchange-correlation energy functional. Using the LSDA together with the experimental lattice parameter is known from earlier results to be an adequate approximation.[20] A basis set consisting of s, p, and d orbitals was used to expand the wave functions within the atomic spheres.

Due to the change in stoichiometry, the formation energy of the defects is calculated using the formula

$$\Delta E = E^{def} - E^{id} + n_{Ni}\mu^0_{Ni} + n_{Mn}\mu^0_{Mn} + n_{Sb}\mu^0_{Sb}, \qquad (1)$$

where E^{def} and E^{id} are the total energies of the supercell with and without a defect. n_i takes into account that when forming the defect, n_i atoms are transferred to or from a chemical reservoir with a chemical potential μ^0_i. In this work the [001]-ordered fcc antiferromagnetic Mn, ferromagnetic fcc Ni, and diamond structure Sb have been chosen as reservoir phases.

In the case of stoichiometric atomic swap defects Eq. (1) is simplified to

$$\Delta E_{swap} = E^{def} - E^{id}. \qquad (2)$$

Competing crystalline phases that might be formed in the alloy preparation process are not taken into account. Charged defects are not considered, and we believe them to be less likely in half-metallic systems than in semiconductors due to the conduction capability of spin-up electrons. Local lattice relaxations around the defects are not considered. We believe that such relaxations might lower the quantitative values of the formation energies by 10%–20%,[21,22] but this will not change the conclusions of this work. Local relaxations are unlikely to influence the defect impact on the half-metallic character of the system. In the case of vacancies this is due to the microscopic impact those defects have on the band structure. In the case of interstitial Ni and Mn the local relaxations are believed to be very small. This is due to the fact that the $C1_b$ crystal structure with an "empty site" is similar to the $L2_1$ structure of the full-Heusler structure. This makes it possible for the material to incorporate extra Ni or Mn without changing the positions of the neighboring ions more than slightly. This is shown by the very small difference in lattice parameter between NiMnSb and the full-Heusler alloy $\mathrm{Ni_2MnSb}$, 3% according to our calculations. Note that some defects that destroy the half-metallicity of NiMnSb might be slightly more affected by the local relaxations. However, we will show that those defects have extremely high formation energies (several electronvolts). This means that even if the formation energies are overestimated due to the neglect of local relaxations by as much as 20%, those defects are unlikely to appear in experimental samples.

In order to confirm the accuracy of the KKR-ASA approach for the systems of interest, we performed the following test calculations: We compared KKR-ASA calculations within the coherent potential approximation[16,17] (CPA) with the CPA calculation within the framework of the more accurate exact muffin-tin orbitals[23,24] (EMTO) scheme. The CPA method is in fact a limiting case of the LSGF method when the local interaction zone is reduced to a single site. In Fig. 1 we present the results of defect energy calculations with the KKR-ASA-CPA, EMTO-CPA, and our supercell KKR-ASA-LSGF method. It is obvious from the figure that the results obtained by the KKR-ASA-CPA method are in good agreement with the EMTO-CPA calculations. This shows that the KKR-ASA scheme is sufficient for the purpose of our studies. However, the figure also shows that the impact of considering local environment effects by using a larger local interaction zone in our LSGF calculations than the single site CPA treatment is considerable. This justifies the usage of the KKR-ASA-LSGF method which is more time consuming as compared to CPA. However, since our total energy calculations omit an analysis of competing crystalline phases as well as neglecting the effects of kinetic barriers and local lattice relaxations, the resulting formation energies are only used for qualitative conclusions about the possibility of the appearance of defects in experiments, rather than quantitative values to be used in predicting exact temperature-dependent concentrations.

When we report on the effect of defects on the magnetic moment we present the change of the magnetic moment per formula unit. In the ground state of pure NiMnSb the moment is predicted[1] to be integer $4.00\mu_B$/f.u., a value that is reproduced in this work.

When we present plots of the density of states (DOS) of the defect supercells we do so by showing the site-projected DOS at the impurities together with the host DOS of NiMnSb. Since we carry out calculations in a dilute regime, the defect is unlikely to change the host DOS more than locally. Previous work on a similar material has shown[25] that impurity states are strongly localized to the impurity site itself so even the local environment is only slightly modified. Our calculations give the same results, and we did not find any case where impurity states which are not localized at the impurity site change the character of the system with respect to the half-metallicity on their own. That is, if the defect destroys half-metallicity, it possesses spin-down states at the Fermi level located at the impurity site. And if the impurity

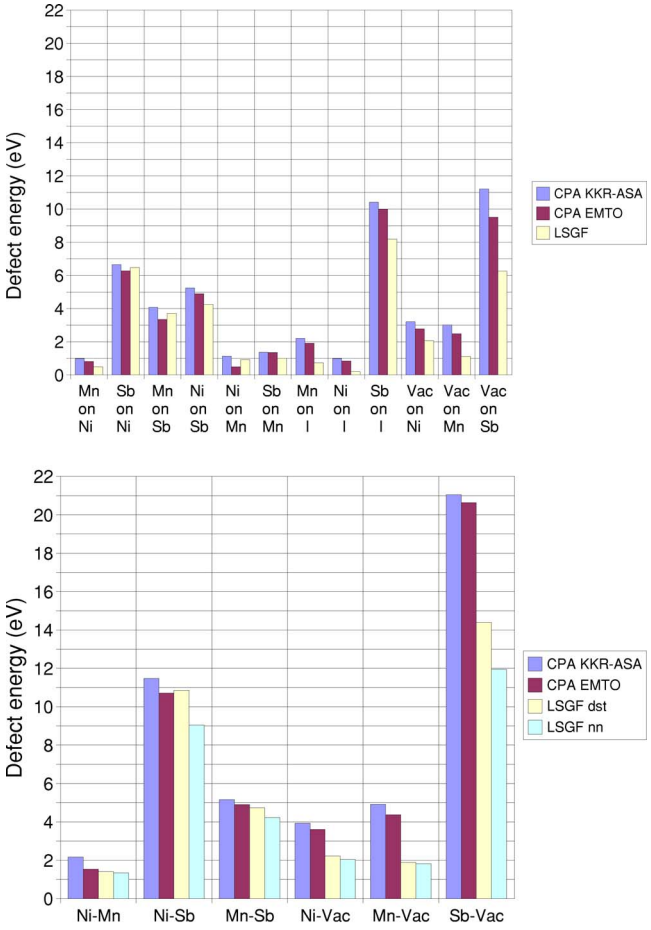

FIG. 1. (Color online) Energies of antisite (top graph) and atomic swap (bottom graph) defects in NiMnSb calculated with three different methods: KKR-ASA-CPA (first), EMTO-CPA (second), and LSGF (third). In addition, for the swap defects the energy of both the distant swap (third) and nearest-neighbor swap (fourth) is shown.

site has a vanishing spin-down DOS at E_F, half-metallicity is kept in the entire supercell. This motivates the way we present the DOS. Since our method of calculating the DOS involves evaluation of the Green's function in the complex energy plane, a small broadening of the states is expected to show up in the DOS pictures.[26] Since this can be crucial in deciding whether a material is half-metallic or not, we have complemented the study of the DOS with counting the number of electrons with each spin within our entire supercell. An integer number of spin-down electrons (and thus an integer number of spin-up electrons as well) is an indication that the system is indeed half-metallic. We do not show the DOS for vacancies because the DOS projection onto the vacant site is so small that therefore it is pointless to present it. However, the vacancies can potentially destroy the half-metallicity and are discussed in the text.

IV. RESULTS AND DISCUSSION

In Table I we report the results of our calculations for the nonstoichiometric defects: the formation energies, the change of the magnetic moment, and the influence on the half-metallicity of NiMnSb in the dilute regime. The defects in the table are sorted according to the formation energy. In Table II we report the same parameters for the atomic swap defects.

TABLE I. Formation energy (in eV), magnetic moment change per formula unit (in μ_B relative to $4\mu_B$), and effect on the spin polarization of antisite defects, interstitials, and vacancies in NiMnSb. Defects are sorted according to their formation energy.

Defect	ΔE	ΔM	Half-metallic
Ni_I	0.20	0	Yes
Mn_{Ni}	0.49	−0.024	Yes
Mn_I	0.73	0.008	Yes
Ni_{Mn}	0.92	−0.056	Yes[a]
Sb_{Mn}	1.01	−0.032	Yes
vac_{Mn}	1.12	−0.056	Yes
vac_{Ni}	2.07	0	Yes
Mn_{Sb}	3.70	0.016	Yes
Ni_{Sb}	4.25	−0.005	No
vac_{Sb}	6.27	−0.014	No
Sb_{Ni}	6.47	0.021	No
Sb_I	8.19	0.021	No

[a]Half-metallic character for NiMnSb with this defect is decided on the grounds of integer number of spin-down electrons in the supercell. See text for discussion.

A. Ni, Mn, and Sb in an interstitial position

We first consider the defects formed by placing an atom on the empty sublattice—that is, at site C with the offset $(\frac{1}{2},\frac{1}{2},\frac{1}{2})$. It is intuitive that the defect with the lowest formation energy is Ni_I with $\Delta E=0.20$ eV. This is so because the full-Heusler alloy Ni_2MnSb actually exists in the corresponding $L2_1$ structure where all the C sites are occupied by Ni atoms. Also the Mn_I defects show a relatively low formation energy (0.73 eV) while putting an Sb atom in the interstitial position takes a huge energy (8.19 eV), rendering the Sb_I defect highly unlikely to appear in the alloy.

We will now turn to the electronic and magnetic properties of the defective NiMnSb system. Since our calculations are made in the dilute regime, the defects are unlikely to affect the DOS of the NiMnSb host more than locally. The defects can anyway destroy the half-metallicity if they induce impurity states for spin-down electrons at the Fermi energy. In Fig. 2 we therefore show the impurity-site DOS (not scaled by concentration) together with the host DOS of NiMnSb (the host DOS is presented as the DOS in one unit cell).

One can easily see that neither Ni_I nor Mn_I destroys the half-metallic properties (manifested by the vanishing spin-down DOS at E_F) in the dilute regime. However, due to the induced states below E_F (but still in the gap) in the case of Ni_I and on both sides of E_F in the case of Mn_I, the defects are likely to destroy the spin-down band gap at high concentrations when the impurity states broaden. This is manifested by

TABLE II. Formation energy (in eV), magnetic moment change per formula unit (in μ_B relative to $4\mu_B$), and effect on the spin polarization of atomic swap defects in NiMnSb. Defects are sorted by formation energy.

	ΔE		ΔM		Half-metallic	
Defect	nn	dst	nn	dst	nn	dst
Ni-Mn swap	1.34	1.41	−0.080	−0.080	Yes[a]	Yes[a]
Mn-vac swap	1.83	1.89	−0.048	−0.048	Yes	Yes
Ni-vac swap	2.04	2.22	0	0	Yes	Yes
Mn-Sb swap	4.23	4.73	−0.011	−0.017	No	Yes
Ni-Sb swap	9.04	10.85	0.005	0.015	No	No
Sb-vac swap	11.95	14.4	−0.009	0.005	No	No

[a]Same as Ni_{Mn}.

the fact that Ni_2MnSb is not predicted to be half-metallic. On the other hand, putting a Sb atom in an interstitial position immediately destroys the half-metallicity because of a peak in the spin-down DOS right at the Fermi level.

One of the interstitial defects with low formation energy, the Mn_I, shows an increase of the average magnetic moment per cell above its value in ideal NiMnSb. It increases the moment by $0.008\mu_B$ per f.u. This can explain the experimentally observed fact that the magnetic moments of some samples are slightly above $4.00\mu_B$.[3,5,13,14] This hypothesis is strengthened by observations that Mn is consumed faster than Ni and Sb in some methods of alloy preparation.[3,13] The Ni_I defect does not show any effect at all on the average magnetic moment of the system. A Sb atom in the energetically unfavorable interstitial position increases the magnetic moment by $0.021\mu_B$ per f.u.

B. Defects at the Ni sublattice

The Mn_{Ni} antisite defect has a formation energy of 0.49 eV. This is slightly lower but comparable with the formation energy of Mn_I. Figure 3 shows the calculated DOS for the Mn_{Ni} and the Sb_{Ni} defects. It is interesting to notice that if a Mn atom occupies a Ni site, the spin-down band gap is not affected at all. This indicates that the defect most probably will not destroy half-metallicity even at high concentrations. It is interesting to notice that $C1_b$-structure MnMnSb with all of the Ni atoms replaced by Mn is also predicted to be half-metallic[27] although it crystallizes in the Cu_2Sb structure which is a normal metal.

The decrease in magnetic moment by $0.024\mu_B$ per f.u. corresponds to a decrease of $3\mu_B$ in the whole supercell. It seems that the removal of three electrons when substituting Mn for Ni is done exclusively from the spin-up band. We will discuss this in more detail in Sec. IV F.

An Sb antisite at the Ni sublattice induces spin-down states at the Fermi level. The vacancy at the Ni sublattice (the DOS is not shown) almost does not affect the band structure. Both the Sb_{Ni} and Ni vacancy have large formation energies, 6.47 and 2.07 eV, respectively, making them unlikely to occur in a NiMnSb sample at substantial concentrations.

C. Defects at the Mn sublattice

The antisite defects at the Mn sublattice all have formation energies around 1 eV. Although a considerable energy, those defects might be formed in alloy preparation if there is a deficiency of Mn. Figure 4 shows that Ni_{Mn} and Sb_{Mn} introduce states in the gap for the spin-down band below the Fermi energy. In the case of Ni_{Mn} it appears to be hard to distinguish if the state crosses E_F, destroying half-metallicity. The uncertanty is due to the numerical broadening of the DOS. However, the number of spin-down electrons in the whole supercell is integer which indicates that half-metallicity is preserved. However, the existence of a state so close to E_F shows that half-metallicity might be lost at higher concentrations. It is known from earlier work[11,15] that the Ni-Mn swap is harmful for the spin-down band gap at slightly higher concentration than the one studied by us. Orgassa *et al.*[11] even concluded that this is due to the presence of Ni at the Mn site rather than Mn at the Ni site, a conclusion confirmed by our calculations.

It is not surprising that the removal of one Mn atom, the carrier of the largest individual moment, reduces the net magnetic moment in the alloy. The Ni_{Mn} defect decreases the magnetic moment by $0.056\mu_B$ per formula unit. This corresponds to a total change in the whole supercell by $-7.0\mu_B$.

D. Defects at the Sb sublattice

Defects that include the Sb sublattice all show high formation energies. This is true for both nonstoichiometric and stoichiometric defects and makes the formation of those defects unlikely. Figure 5 shows the DOS at the Ni_{Sb} and Mn_{Sb} defects. Mn atoms at the Sb sublattice induce spin-down states in the gap but below the Fermi level, thus preserving half-metallic properties in the dilute regime. On the other hand, the presence of Ni atoms at the Sb sublattice as well as Sb vacancies destroys half-metallicity by creating spin-down states just at the Fermi level. The Mn_{Sb} defect increases the magnetic moment while the Ni_{Sb} and Vac_{Sb} defects decrease it.

E. Atomic swap defects

The study of the atomic swap defects is interesting in many ways. The defects including swaps of distant atoms

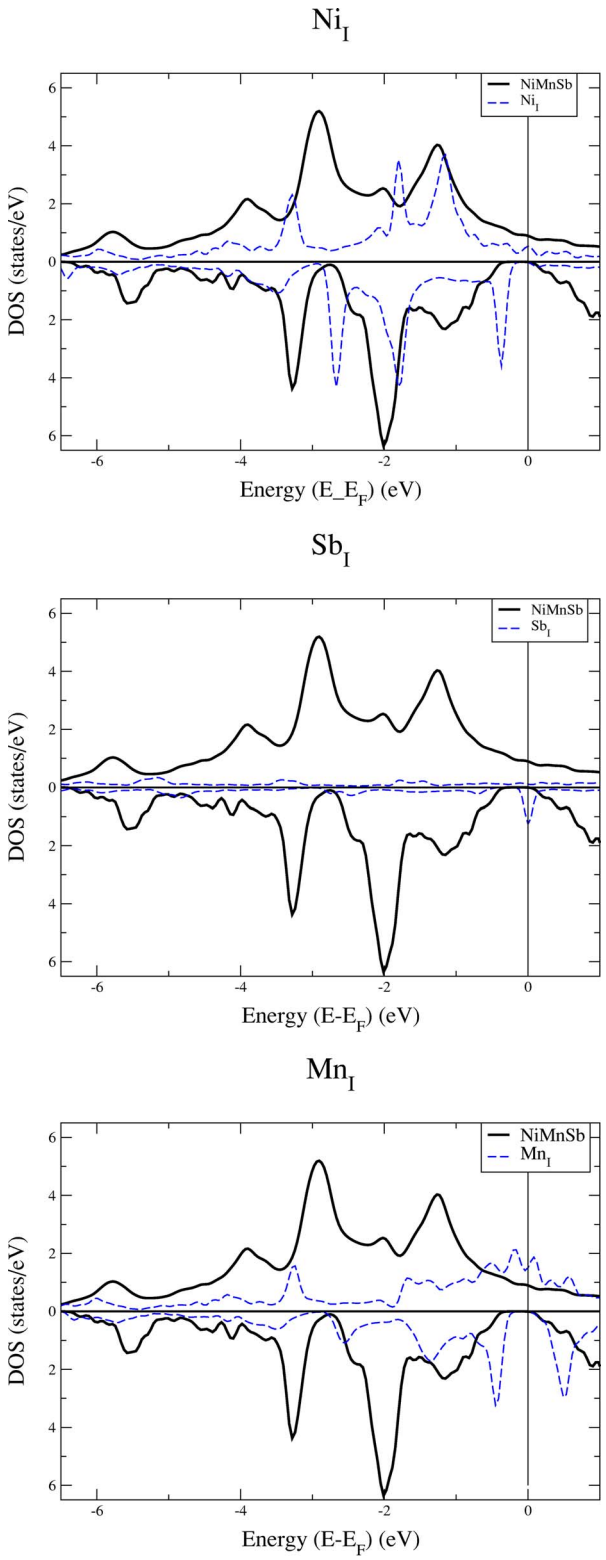

FIG. 2. (Color online) Spin-up DOS (above 0) and spin-down DOS (below 0) at the sites occupied by Ni_I, Mn_I, and Sb_I defects (dashed line, states/eV/atom) together with the host DOS of NiMnSb (solid line, states/eV/f.u.).

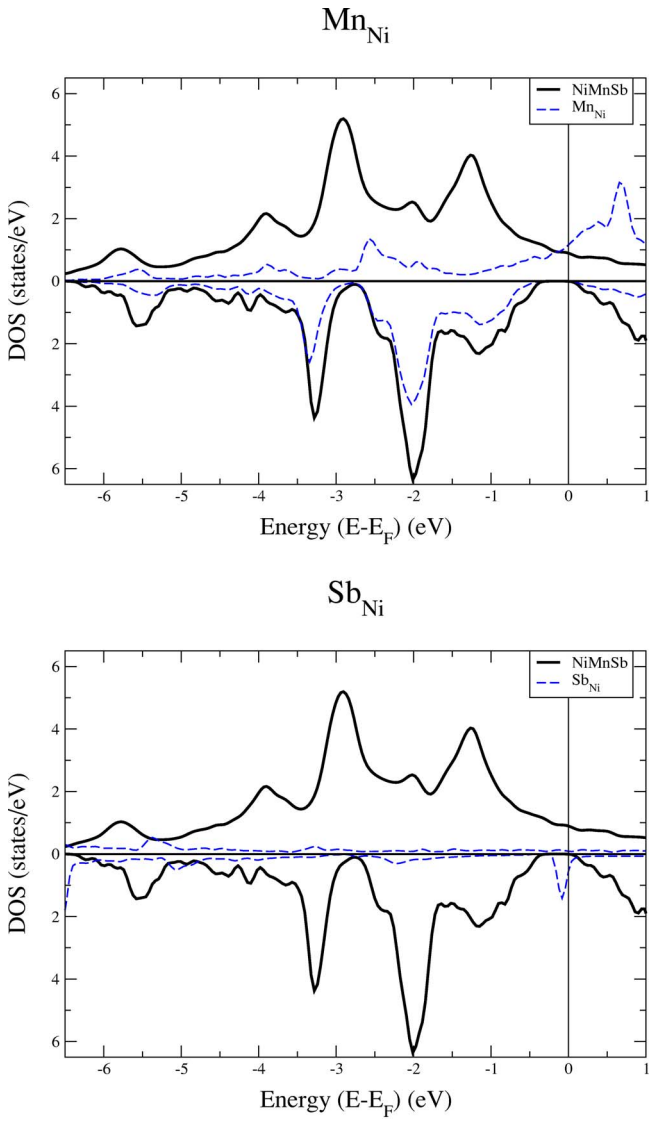

FIG. 3. (Color online) Spin-up DOS (above 0) and spin-down DOS (below 0) at the sites occupied by Mn_{Ni} and Sb_{Ni} defects (dashed line, states/eV/atom) together with the host DOS of NiMnSb (solid line, states/eV/f.u.).

can be seen as a combination of two antisite defects. This is so because the considerable distance between the defected sites makes a strong interaction between them unlikely. On the other hand, when interchanging neighboring atoms there is an interaction between the defect sites that might alter the properties of the system. Atomic swap defects have also been studied before, so a comparison with previous theoretical works can be done. The DOS of the atomic swap defects are presented in Figs. 6 and 7.

Our results show the anticipated similarities between the swap of distant atoms and the corresponding antisite defects. When the formation energy, magnetic moment change, and DOS are considered the distant atom swap corresponds to a combined effect of two antisite defects. The neighboring atom swaps show a lower formation energy than the corresponding distant swaps. This means that in NiMnSb there is an attraction between any two antisite defects that corresponds to a swap of atoms: for example, a $Ni_{Sb}Sb_{Ni}$ pair.

In one case the swaps of distant and nearest-neighbor atoms have a different effect on the spin polarization at the

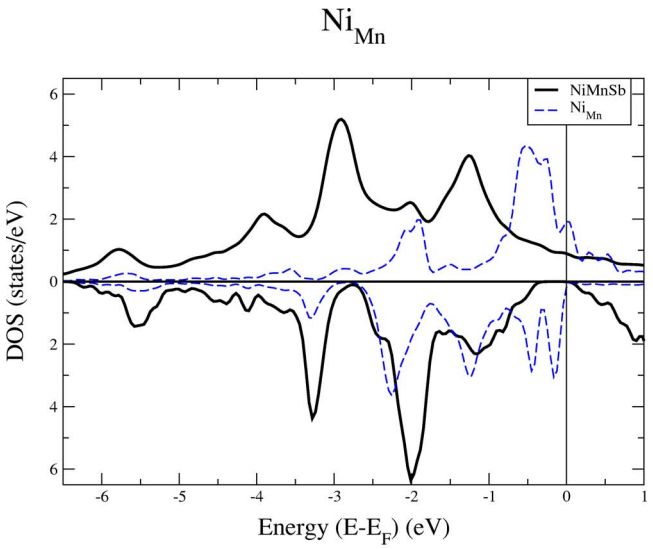

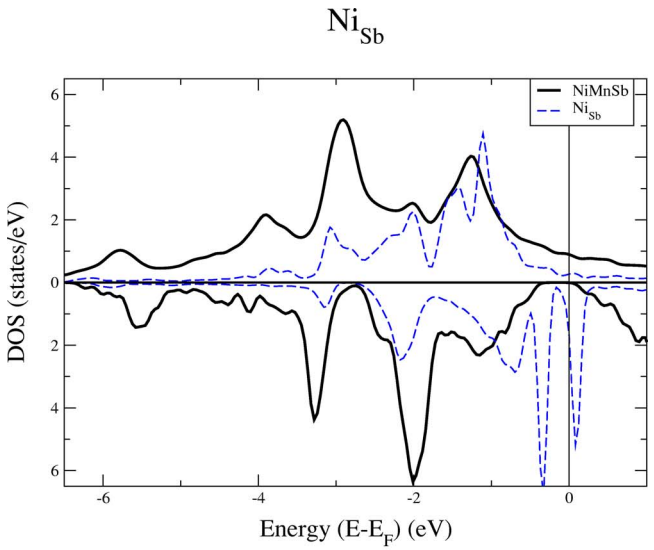

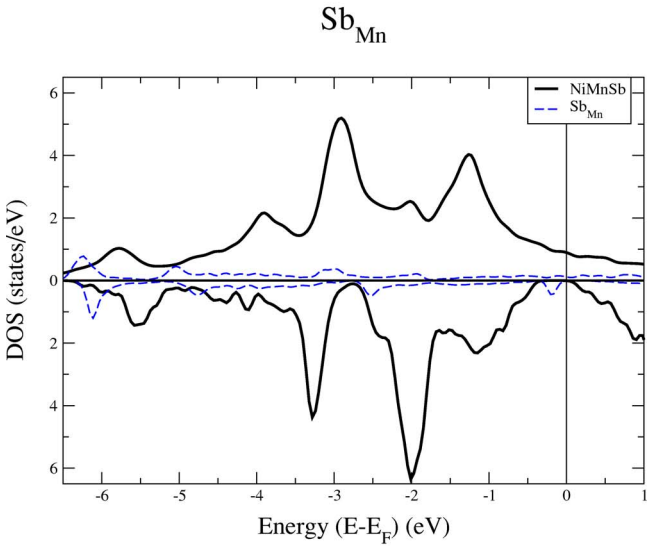

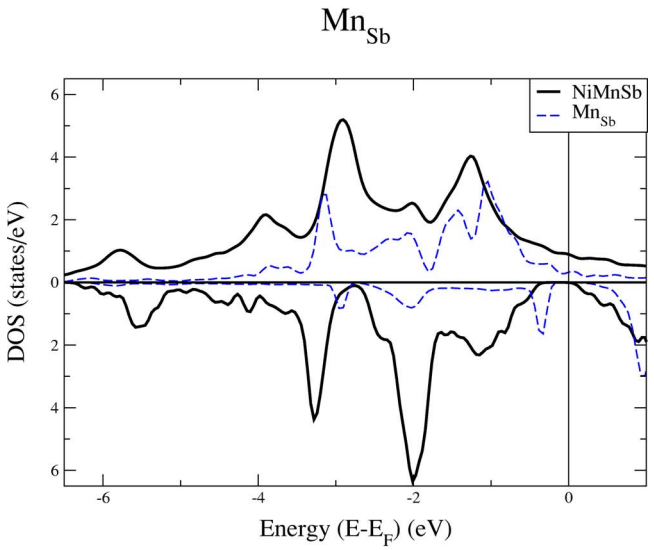

FIG. 4. (Color online) Spin-up DOS (above 0) and spin-down DOS (below 0) at the sites occupied by Ni_{Mn} and Sb_{Mn} defects (dashed line, states/eV/atom) together with the host DOS of NiMnSb (solid line, states/eV/f.u.).

FIG. 5. (Color online) Spin-up DOS (above 0) and spin-down DOS (below 0) at the sites occupied by Ni_{Sb} and Mn_{Sb} defects (dashed line, states/eV/atom) together with the host DOS of NiMnSb (solid line, states/eV/f.u.).

Fermi level. In the case of a neighboring Mn-Sb swap a spin-down state appears at the Fermi level, thus destroying the half-metallicity. In the case of more distant Mn-Sb swaps, this state is shifted at the Fermi level.

Three different atomic swap defects were previously studied within the CPA sheme by Orgassa *et al.*[11,12] These are the Ni-Mn swap and two defects that can be seen as a combination of Ni-vacancy and Mn-vacancy swaps as well as Mn-vacancy and Sb-vacancy swaps. Where a comparison is possible our results are in fair agreement with those of Refs. 11 and 12. The only difference is that the impurity states induced by the Sb-vacancy swap destroys the spin-down band gap in our case already at low concentration (0.8%) while in Refs. 11 and 12 this requires concentrations between 1% and 5%. A recent article by Attema *et al.*[15] presents a short summary of their results for swap defects as well as the Ni_I and vac_{Ni} defects. They only present the calculated formation energy for one defect, the Ni-Mn swap, which is 2.88 eV. This is twice our value. The difference might be due to the fact that the defect concentration in Ref. 15 is 3% which is higher than in our simulations. Because of the broadening of the spin-down states below E_F, the half-metallic character of the system is destroyed at high concentrations, which should substantially increase the energy of the system. If one compares our results for the effect of defects on the half-metallicity of NiMnSb with those in Ref. 15, they agree for 10 out of 14 cases. Besides the Ni-Mn swaps mentioned above we obtain different results for the nearest-neighbor Ni-Sb swaps and nearest-neighbor Sb-vacancy swaps. We find a finite spin-down DOS at E_F (small in the case of Sb-vacancy swaps but large in the case of Ni-Sb swaps) while Ref. 15 claims that the half-metallicity is preserved.

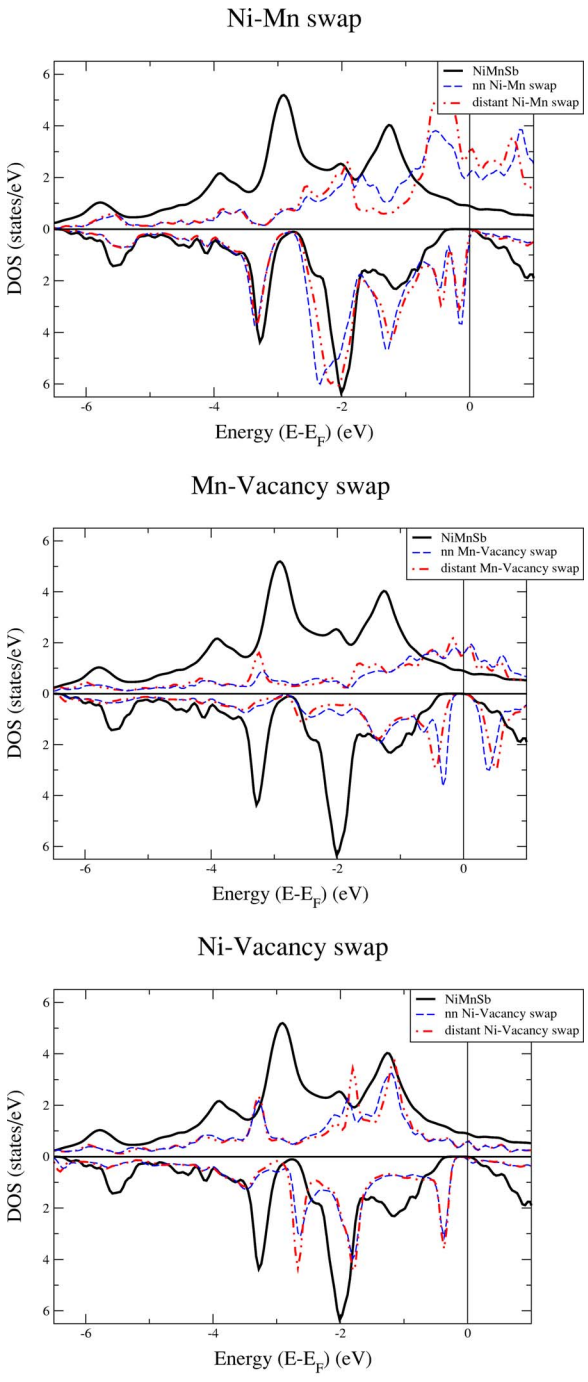

FIG. 6. (Color online) Spin-up DOS (above 0) and spin-down DOS (below 0) of the defective sites in the Ni-Mn, Mn-vac, and Ni-vac swap defects (states/eV/defect pair) together with the host DOS of NiMnSb (solid line, states/eV/f.u.). Nearest-neighbor swaps are shown with dashed lines while distant swaps are the dash-dotted lines.

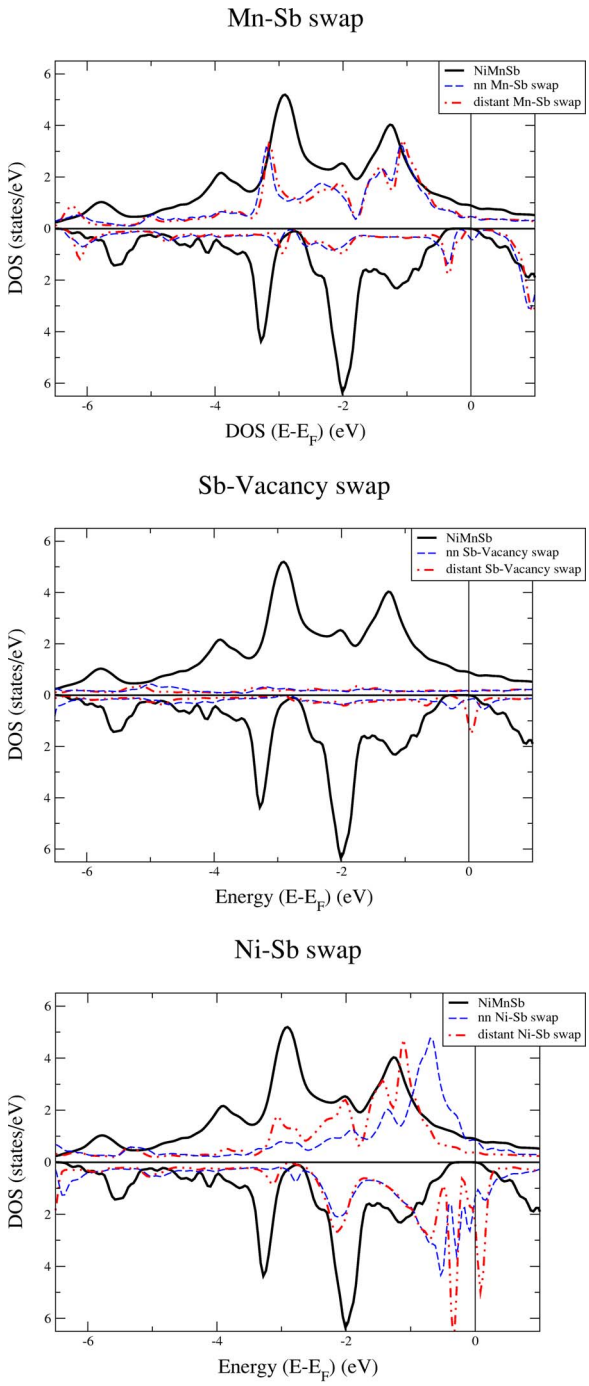

FIG. 7. (Color online) Spin-up DOS (above 0) and spin-down DOS (below 0) of the defective sites in the Mn-Sb, Ni-Sb, and Sb-vac swap defects (states/eV/defect pair) together with the host DOS of NiMnSb (solid line, states/eV/f.u.). Nearest-neighbor swaps are shown with dashed lines while distant swaps are the dash-dotted lines.

F. Discussion

When we now have the results of the calculations of the defects it is possible to discuss why some defects destroy the half-metallicity while others do not.

The origin of the gap in the spin-down channel is the covalent hybridization between the lower-energy *d* states of the high-valent Ni atoms and the higher-energy *d* states of the lower-valent Mn atom, leading to the formation of bonding and antibonding bands.[20] NiMnSb have 22 valence electrons per f.u., leading to population of both the bonding and antibonding states. Consequently the Stoner criterion is fulfilled which puts NiMnSb into a ferromagnetic state. The half-metallic configuration is the energetically most favor-

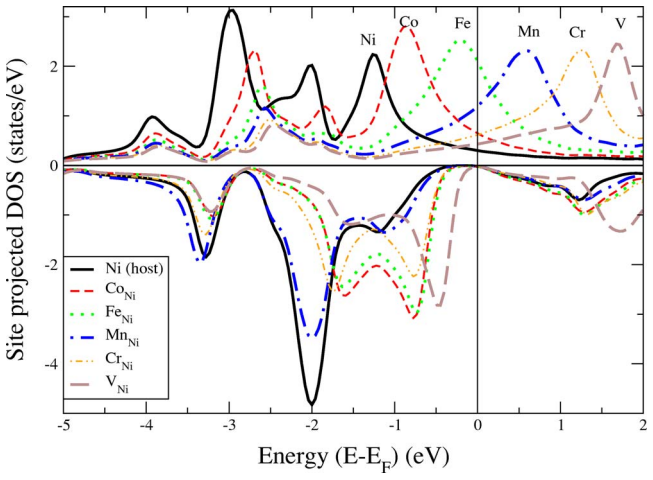

FIG. 8. (Color online) The site-projected DOS of transition-metal impurities on the Ni site in NiMnSb. Note that the gap in the spin-down band is preserved while the spin-up band performs a shift.

able state due to the presence of the gap in the minority band.[20] In the ground state three transition-metal d electrons hybridize with the s and p states of Sb. This leaves 14 valence d electrons that occupies the five spin-up and five spin-down bonding states and four spin-up antibonding states. The spin-up bonding and antibonding states are of almost equal Ni and Mn character while the bonding spin-down states are mostly of Ni character and the unoccupied antibonding spin-down states are of Mn character.[20]

This information makes it possible to understand what happens when Ni and Mn are put on each other's sublattices. When Mn sits at the Ni sublattice simply three fever electrons occupy the antibonding spin-up states. In this way the spin-down band preserves the energetically favorable gap at E_F and have the same occupancy where the five bonding d states are filled below the band gap. On the other hand, when Ni sits on the Mn site three extra valence d electrons are present comparing to the ideal unit cell. Since there is only room for one more electron in the spin-up band, some electrons have to be accommodated in the antibonding spin-down band. One would expect this to destroy half-metallicity. However, the energetically most favorable situation turns out to be a state where two spin-up electrons are moved to the spin-down channel and together with three extra electrons completely fill the antibonding part of the spin-down band. This preserves the half-metallicity in a very dilute regime. The scenario described above can be clearly seen in Figs. 4 and 6, where the DOS for both the Ni_{Mn} antisite defect and the Ni-Mn swaps are shown.

The investigation of the Mn_{Ni} and Ni_{Mn} defects sugests that the spin-down band is quite insensitive to the chemical disorder at the Ni and Mn sublattices in the dilute regime. To test this we performed KKR-ASA-CPA calculations of a series of low-concentration transition-metal impurities at the Ni sublattice. In Fig. 8 we show the density of states for the impurity site at the Ni sublattice occupied by Co, Fe, Mn, Cr, and V, respectively. It is obvious that the spin-down band gap is preserved and that the spin-up channel shows a typical metallic rigid band shift. The result is that those defects behave like "Slater-Pauling-defects," which means that the magnetic moment has a strictly linear dependence on the electron number of the impurity. A decrease in electron number by 1 when going from Ni to Co leads to a decrease of the magnetic moment by $1\mu_B$, etc.

Other defects show a more complicated behavior since the difference between the ideal and defective unit cells is larger. When Ni or Mn is in the interstitial position a covalent hybridization between the d states of the defect and the d states of the Mn neighbors occurs. In the case of Mn_I the bonding and antibonding states are clearly visible with the gap between them right at the Fermi level. In the case of Ni_I only the spin-down bonding d states are visible in the plot since the antibonding states are of mainly Mn character positioned right above E_F.

Putting a defect at the Sb sublattice makes a large change in the electronic structure which is reflected by high formation energies. However, the local environment of the Sb site is similar to that of the Mn site which is seen in the similarities between the impurity DOS of the Ni_{Sb} and Ni_{Mn} defects. In the case of the Mn_{Sb} antisite the Mn-Ni hybridization occurs, and even though the splitting between bonding and anti-bonding spin-down states is smaller than in the ideal structure, the gap at E_F is preserved.

When Sb atoms are displaced to Ni or interstitial positions a single d-character state appears right at E_F. The nature of this state is not entirely clear but a hybridization with d states of the neighboring Mn atoms is likely.

The vacancies at the Ni and Mn sites show only small effects on the DOS preserving half-metallicity in both cases. However, replacing the Sb atom with a vacancy creates a p-dominated state in the spin-down band gap, crossing the Fermi level. This can be seen as the effect of removing the low-energy s and p bands of Sb which accommodates Ni and Mn valence electrons.

V. CONCLUSIONS

We carried out first-principles calculations of all 6 possible intrinsic antisite defects in NiMnSb, as well as 3 interstitials, 3 vacancy defects, and 12 atomic swap defects by means of a KKR-ASA locally self-consistent Green's-function method. We have found that the defect formation energies range from 0.2 eV (Ni_I) to 14.4 eV (distant Sb-vacancy swap).

All the defects with formation energies below 4 eV keep the half-metallic property of bulk NiMnSb. The defects that damage half-metallicity and induce states in the spin-down band gap at the Fermi level, causing a reduction of spin polarization of conduction electrons show higher formation energies. Also there exists a category of defects like Sb_{Mn} and vac_{Mn} which induce electronic states in the minority-spin band gap, though the states do not cross the Fermi level in the dilute regime. Our results indicate that the half-metallic character of NiMnSb is unlikely to be destroyed by low concentrations of defects. The main threat would be the Ni_{Mn} defect, which might destroy the half-metallicity at moderately low concentrations.

We have found that some defects, most interestingly Mn_I, cause an *increase* of the magnetic moment. This might explain the experimentally observed magnetic moments which are higher than the theoretical value for ideal NiMnSb. A defective sample of NiMnSb can show both higher and lower magnetic moments than $4.00\mu_B$. This indicates that there is no easy way to determine the structural quality or even less the spin polairization at the Fermi level of a NiMnSb sample solely from measurements of the saturation magnetization.

The spin-down band with its characteristic gap at the Fermi level seems to be quite resistant against chemical disorder at the Ni and Mn sublattices. In fact, when antisite defects with gradually lower electron number are present at the Ni site the spin-down band keeps the same occupation number while the spin-up band loses electrons. This leads to a "Slater-Pauling behavior" of the magnetic moments of those defects. Half-metallicity can even be preserved in the case of defects which have a surplus of valence electrons that cannot be fitted in the antibonding spin-up states. This can be exemplified by the Ni_{Mn} antisite defect.

ACKNOWLEDGMENTS

We are grateful to the Swedish Research Council (VR) and The Swedish Foundation for Strategic Research (SSF) for financial support.

*Also at IPMC-Faculty of Basic Science, Swiss Federal Institute of Technology Lausanne (EPFL), 1015 Lausanne, Switzerland. Electronic address: bjoal@ifm.liu.se

[1] R. A. de Groot, F. M. Mueller, P. G. van Engen, and K. H. J. Buschow, Phys. Rev. Lett. **50**, 2024 (1983).
[2] K. E. H. M. Hanssen, P. E. Mijnarends, L. P. L. M. Rabou, and K. H. J. Buschow, Phys. Rev. B **42**, 1533 (1990).
[3] M. J. Otto, R. A. M. van Woerden, P. J. van der Valk, J. Wijngaard, C. F. van Bruggen, C. Haas, and K. H. J. Buschow, J. Phys.: Condens. Matter **1**, 2341 (1989).
[4] J. S. Moodera and D. M. Mootoo, J. Appl. Phys. **76**, 6101 (1994).
[5] R. B. Helmholdt, R. A. de Groot, F. M. Mueller, P. G. van Engen, and K. H. J. Buschow, J. Magn. Magn. Mater. **43**, 249 (1984).
[6] J. P. Nozires, C. Hordequin, and J. Pierre, J. Magn. Magn. Mater. **183**, 225 (1998).
[7] J. A. Caballero, A. C. Reilly, Y. Hao, J. Bass, W. P. Pratt, Jr., F. Petroff, and J. R. Childress, J. Magn. Magn. Mater. **198**, 55 (1999).
[8] R. J. Soulen, Jr. *et al.*, Science **282**, 85 (1998).
[9] A. Debernardi, M. Peressi, and A. Baldereschi, Mater. Sci. Res. **23**, 743 (2003).
[10] G. A. deWijs and R. A. de Groot, Phys. Rev. B **64**, 020402(R) (2001).
[11] D. Orgassa, H. Fujiwara, T. C. Schulthess, and W. H. Butler, Phys. Rev. B **60**, 13237 (1999).
[12] D. Orgassa, H. Fujiwara, T. C. Schulthess, and W. H. Butler, J. Appl. Phys. **87**, 5870 (2000).
[13] S. Gardelis, J. Androulakis, J. Giapintzakis, S. K. Clowes, Y. Bugoslavsky, W. R. Branford, Y. Miyoshi, and L. F. Cohen, J. Appl. Phys. **95**, 8063 (2004).
[14] L. Ritchie, G. Xiao, Y. Ji, T. Y. Chen, C. L. Chien, M. Zhang, J. Chen, Z. Liu, G. Wu, and X. X. Zhang, Phys. Rev. B **68**, 104430 (2003).
[15] J. J. Attema, C. M. Fang, L. Chioncel, G. A. de Wijsand, A. I. Lichtenstein, and R. A. de Groot, J. Phys.: Condens. Matter **16**, 5517 (2004).
[16] I. A. Abrikosov and H. L. Skriver, Phys. Rev. B **47**, 16532 (1993).
[17] A. V. Ruban and H. L. Skriver, Comput. Mater. Sci. **15**, 119 (1999).
[18] I. A. Abrikosov, A. M. N. Niklasson, S. I. Simak, B. Johansson, A. V. Ruban, and H. L. Skriver, Phys. Rev. Lett. **76**, 4203 (1996).
[19] I. A. Abrikosov, S. I. Simak, B. Johansson, A. V. Ruban, and H. L. Skriver, Phys. Rev. B **56**, 9319 (1997).
[20] I. Galanakis, P. H. Dederichs, and N. Papanikolaou, Phys. Rev. B **66**, 134428 (2002).
[21] P. A. Korzhavyi, I. A. Abrikosov, B. Johansson, A. V. Ruban, and H. L. Skriver, Phys. Rev. B **59**, 11693 (1999).
[22] D. A. Andersson and S. I. Simak, Phys. Rev. B **70**, 115108 (2004).
[23] O. Andersen, O. Jepsen, and G. Krier, *Lectures on Methods of Electronic Structure Calculation* (World Scientific, Singapore, 1994), pp. 63–124.
[24] L. Vitos, I. A. Abrikosov, and B. Johansson, Phys. Rev. Lett. **87**, 156401 (2001).
[25] S. Picozzi, A. Continenza, and A. J. Freeman, Phys. Rev. B **69**, 094423 (2004).
[26] N. V. Skorodumova, S. I. Simak, I. A. Abrikosov, B. Johansson, and Y. K. Vekilov, Phys. Rev. B **57**, 14673 (1998).
[27] R. A. de Groot, Physica B **172**, 45 (1991).